



Iranian Research Organization
for Science and Technology
(IROST)

Advances
Environmental
Technology



Journal home page: <https://aet.irost.ir>

The impact of annealing temperature on photocatalytic degradation performance of rhodamine B by montmorillonite/zinc-oxide nanocomposite

Bang Tam Thi Dao ^{a,b}, Van Dung Hoang ^{b,c}, Trung Do Nguyen ^{a,c}, Hon Nhien Le ^{a,c}, Huu Truong Nguyen ^{b,c}, Chi-Nhan Ha-Thuc ^{a,c,*}

^a Faculty of Materials Science and Technology, University of Science, Ho Chi Minh City, Vietnam - 227 Nguyen Van Cu Street, Ward 4, District 5, Ho Chi Minh City, 700000, Viet Nam

^b Laboratory of Advanced Materials, University of Science, Ho Chi Minh City, Vietnam - 227 Nguyen Van Cu Street, Ward 4, District 5, Ho Chi Minh City, 700000, Viet Nam

^c Vietnam National University, Ho Chi Minh City, Vietnam - Linh Trung Ward, Thu Duc District, Ho Chi Minh City, 700000, Viet Nam

ARTICLE INFO

Document Type:
Research Paper

Article history:
Received 30 October 2023
Received in revised form
9 July 2024
Accepted 10 July 2024

Keywords:
Photocatalytic Degradation
Rhodamine B
Montmorillonite/Zinc-Oxide
(MMT/ZnO) nanocomposite
rhB Degradation Efficiency
Chromophore Structure

ABSTRACT

This paper investigates the impact of annealing temperature on the photocatalytic degradation efficiency of rhodamine B (rhB) using a montmorillonite/zinc-oxide (MMT/ZnO) nanocomposite. The MMT/ZnO nanocomposites, synthesized through a chemical method, are annealed for one hour at 300°C, 500°C, and 700°C. The study involves a comprehensive analysis of sample composition, surface morphology, and structure using various analytical methods, including Energy Dispersive X-ray Spectroscopy (EDX), Scanning Electron Microscopy (SEM), X-ray Diffraction (XRD), Brunauer-Emmett-Teller (BET) analysis, and Fourier Transform Infrared Spectroscopy (FTIR). RhB degradation efficiency is assessed by monitoring changes in dye concentration in the solution after exposure to UVC radiation, measured with UV-Vis spectroscopy. By-products resulting from the photocatalysis process are identified through LCMS analysis. The results demonstrate that MMT/ZnO annealed at 500°C (referred to as MZ@500) exhibits the highest capability for rhB decomposition, achieving a remarkable 95.5% degradation efficiency with 10 ppm of rhB and 0.1 g/L of MZ@500. Furthermore, this composite effectively fragments the dye's chromophore structure into smaller, ring-broken compounds.

1. Introduction

Montmorillonite (MMT) is the main component of bentonite, a naturally occurring clay mineral that belongs to the smectite group. Its molecular formula is represented as $(\text{Na}, \text{Ca})_{0.33}(\text{Al},$

$\text{Mg})_2(\text{Si}_4\text{O}_{10})(\text{OH})_2 \cdot n\text{H}_2\text{O}$ [1-2]. The fundamental structural unit of montmorillonite mineral comprises a single alumina sheet nestled between two silica sheets, adopting a 2:1-type arrangement. Hydrogen bonds facilitate the connection between the oxygen atoms at the tips of each silica sheet

*Corresponding author Tel.: +84 90 6628359

E-mail: htcnhan@hcmus.edu.vn

DOI: 10.22104/AET.2024.6572.1799

COPYRIGHTS: ©2024 Advances in Environmental Technology (AET). This article is an open access article distributed under the terms and conditions of the Creative Commons Attribution 4.0 International (CC BY 4.0) (<https://creativecommons.org/licenses/by/4.0/>)

and the OH ions on both sides of the alumina sheet. This bond's notable strength contributes to the overall stability of the basic structural unit within the montmorillonite mineral [3, 4]. Montmorillonite (MMT) is renowned for its unique properties, particularly its ability to swell and adsorb substances. Consequently, MMT has garnered significant attention in the realm of water purification, particularly in the context of water environments contaminated with both inorganic and organic impurities [5-10]. However, adsorption alone is insufficient for effectively removing azo dyes. Azo dyes, including compounds like rhodamine B, Disperse Orange 1, and Basic Blue 3, among others, belong to the category of organic compounds characterized by the R-N=N-R' functional group, where R and R' typically represent aryl and substituted aryl groups [11]. These synthetic colorants present a significant challenge for conventional water treatment methods because their complex degradation processes can result in the formation of even more toxic byproducts [12-14]. Therefore, it's crucial to engage in research and innovate natural materials that effectively remove synthetic azo pigments. Previous publications worldwide, as well as our research [14-18], have confirmed that porous heterostructures based on clay minerals are gradually becoming potential alternative materials in the field of removing organic pollutants from wastewater solutions. Some metal oxides are commonly modified into MMT, including ZnO, TiO₂, ZnS, MoS₂, and CdS. These semiconductor photocatalysts can produce hydroxyl radicals when activated by a light source [19, 20]. Among all photocatalysts, ZnO (IIBVIA) is currently widely researched for environmental purification due to its numerous advantages, such as a wide bandgap (3.3 eV), ease of synthesis, non-toxicity, and environmental friendliness. However, ZnO has some disadvantages that limit its photocatalytic efficiency, such as a small surface area, low adsorption capacity, and recombination of photogenerated electron-hole pairs [21-23]. Therefore, the synthesis of MMT/ZnO nanocomposites aims to combine the advantages of both ZnO and MMT while mitigating the drawbacks of these two materials. This helps enhance the efficiency of adsorption and

photodegradation of organic pollutants in wastewater.

In our recent study [17], ZnO nanoparticles were successfully immobilized on the surface and within the interlayer spaces of MMT sheets, forming a house-of-cards structure. Various conditions affecting photocatalytic efficiency, such as light source, catalyst dosage, initial dye concentration, solution pH, and the presence of inorganic and organic scavengers, have been explored in our research and prior studies by other authors. Despite these efforts, the impact of annealing temperature on the photodegradation efficiency of rhB by MMT/ZnO remains unexamined.

Theoretical studies indicate that the adsorption and swelling capacity of MMT decreases with increasing calcination temperature, with significant structural disruption occurring when the temperature exceeds 700-750°C. Given that the adsorption properties of MMT significantly influence the photodegradation efficiency of the MMT/ZnO nanocomposite, understanding the effect of calcination temperature is crucial. This research aims to clarify the influence of calcination temperature on the photodegradation efficiency of rhB by MMT/ZnO through rigorous analytical and experimental methods. It is essential to conduct thorough research to enhance our understanding of these interactions and optimize the performance of MMT/ZnO nanocomposites in photocatalytic applications.

2. Materials and methods

All the chemicals used in this study are of analytical grade, originating from Germany, and did not require further purification before use: Zn(NO₃)₂·6H₂O (≥ 99.0%), C₂H₅OH (≥ 99.8%), rhodamine B (C₂₈H₃₁ClN₂O₃, ≥ 95.0%), NaCl (≥ 99.5%), KOH (≥ 99.8%), and (C₆H₇NaO₆)_n (≥ 99.0%). The bentonite is mined in Lam Dong Province, Vietnam.

2.1. Purify MMT from bentonite

The steps for purifying MMT from bentonite follow the same procedures outlined in our previous publications on MMT [1, 3, 5, 17, 18]. In this process, MMT was dispersed in DI water. NaCl was added to the mixture and stirred for 24 hours. The mixture was allowed to settle; then, it was centrifuged and washed multiple times with ethanol and deionized

water to remove impurities from the bentonite. The final solid obtained after drying at 60°C for 24 hours will yield purified MMT.

2.2. Synthesis of zinc oxide nanoparticles (ZnO_{NP})

The steps in the ZnO_{NP} synthesis process were conducted in the same manner as described in our recent publication [17]. Specifically, zinc nitrate hexahydrate and potassium hydroxide were separately dissolved in distilled water. The potassium hydroxide solution was slowly added to the zinc nitrate hexahydrate solution. The mixture was stirred until it turned white. The solid obtained was centrifuged and washed several times with ethanol. Subsequently, it was annealed for one hour to obtain ZnO_{NP} at different temperatures: $ZnO@300$, $ZnO@500$, and $ZnO@700$.

2.3. Synthesis of montmorillonite/zinc oxide nanocomposite (MMT/ ZnO)

The steps in the MMT/ ZnO synthesis process were performed similarly to our recent publication [17]. First, MMT was dispersed in distilled water using a stirring machine (A). Next, zinc nitrate hexahydrate and sodium alginate were dissolved separately in equal amounts of distilled water; then, they were mixed together (B). Then, (A) was added to (B) and stirred for 24 hours. Afterward, the mixture was centrifuged and washed several times with ethanol and distilled water to obtain MMT/ ZnO . Finally, MMT/ ZnO was annealed for one hour at 300°C, 500°C, and 700°C, corresponding to the labels $MZ@300$, $MZ@500$, and $MZ@700$.

2.4. Characterization methods

The elemental composition of the sample was analyzed using EDX (HORIBA H-7593, Horiba, Japan), and its surface morphology was examined using SEM (Hitachi Co., Japan). Crystallographic characteristics and bonding vibrations were examined through XRD (D2-PHASER, Bruker, Germany) employing CuK scattering at 40 kV and 40 mA, with a scanning speed of 0.030°/s within the 5°-80° range, as well as FTIR. The surface texture, pore volume, and pore diameter of the samples were determined using BET (Brunauer-Emmett-Teller), with N_2 adsorption-desorption isotherms collected at 77.3 K using a Nova 1000e instrument (Quanta chrome). Additionally, the surface area of the samples was analyzed using the

Barrett-Joyner-Halenda (BJH) method. The adsorption efficiency and photocatalytic performance of rhB were determined using UV-Vis spectroscopy (Jasco V-670, Jasco International Co., Japan) in the 400-700 nm range. Byproducts following the photodegradation of rhB were identified using the LC-MS method (Waters Xevo TQS, USA, with a Waters BEH C18 (2.1 × 1.7 × 50 mm) column).

2.5. Adsorption and photocatalytic experiments

This study's experimental procedures on adsorption and photocatalysis closely followed previous literature and were conducted in a closed chamber [15,16]. Specifically, 10 mg of photocatalytic material was introduced into a 100 mL solution containing 10 ppm rhB. Initially, the mixture underwent magnetic stirring in the absence of UVC light for one hour to attain adsorption-desorption equilibrium. Subsequently, the UVC lamp was activated, and the mixture was continuously stirred for 210 minutes. At 30-minute intervals, 5 mL of the solution was centrifuged and analyzed using UV-Vis spectroscopy. The performance of each case was assessed using formula (1) [19-21], with the total efficiency being the sum of the efficiencies of adsorption and photocatalysis.

$$H\% = \frac{C_o - C}{C_o} \times 100 \quad (1)$$

where C_o is the initial dye concentration and C is the dye concentration at time t .

3. Results and discussions

3.1. Structural properties of photocatalysts

The surface morphology of ZnO_{NP} and the MMT/ ZnO nanocomposites at different calcination temperatures are depicted in Figure 1. As the calcination temperature rose, it was noticeable that the crystal size increased because of crystalline growth occurring during the calcination process [22-24]. The average particle size of ZnO_{NP} formed at calcination temperatures of 300°C, 500°C, and 700°C was approximately 50-100 nm, 120-200 nm, and 400-500 nm, respectively [25, 26]. Our recent publications described the surface of MMT as flake-like and organized in layers [27, 28]. It was observed that the surface of the MMT/ ZnO nanocomposites became more tightly packed as

the calcination temperature increased due to the influence of the agglomeration phenomenon.

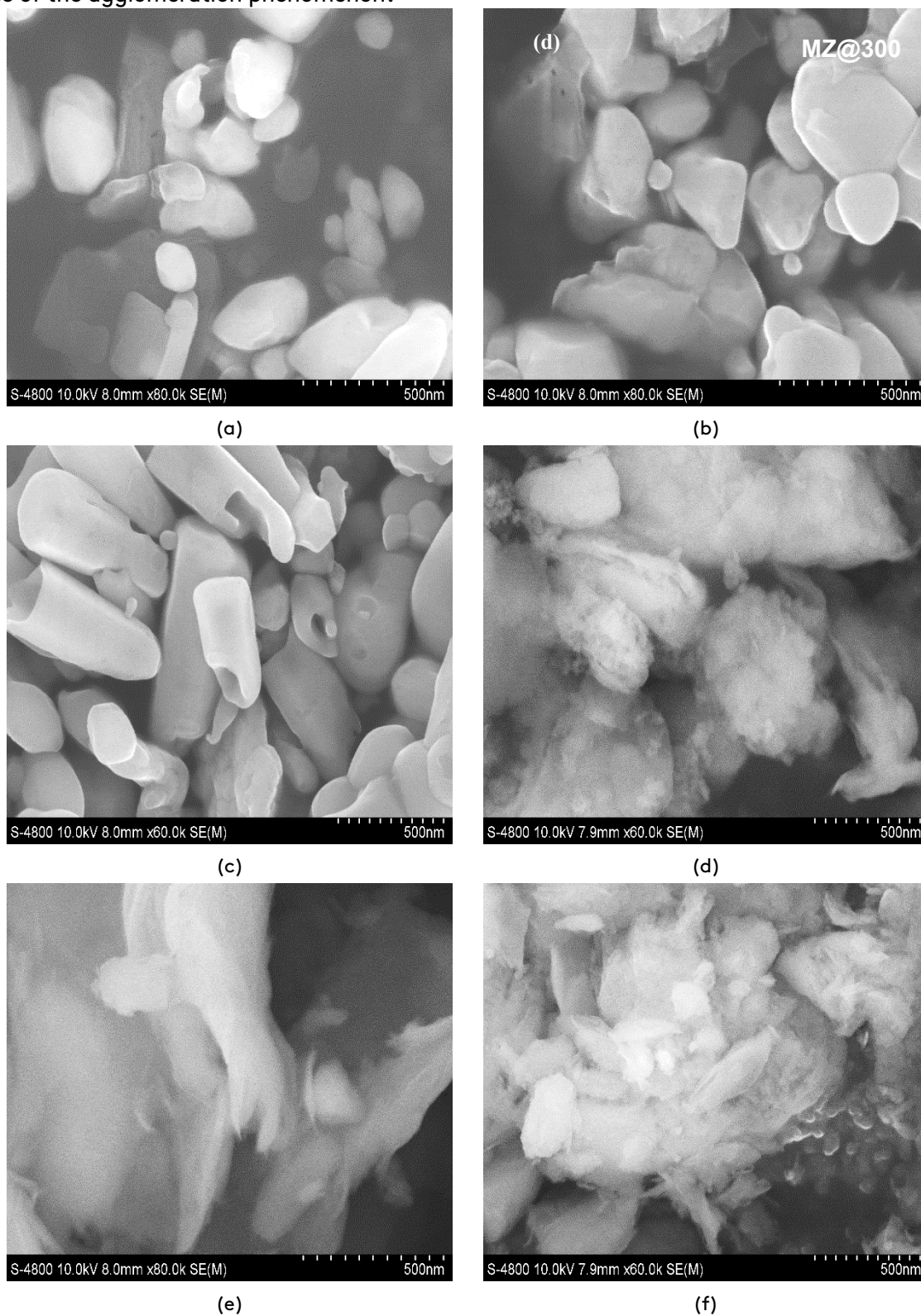


Fig. 1. FESEM images of (a) ZnO@300, (b) ZnO@500, (c) ZnO@700, (d) MZ@300, (e) MZ@500, and (f) MZ@700.

Figures 2a, 2b, and 2c represent the EDX spectra of MZ@300, MZ@500, and MZ@700, respectively. Previous publications and other studies [17, 18] have affirmed that MMT consists of multiple elements, including potassium (K), calcium (Ca), oxygen (O), silicon (Si), magnesium (Mg), sodium (Na), iron (Fe), and aluminum (Al). Therefore, the composition of the nanocomposites, in addition to

the elements of MMT, also included the element Zn, with nearly equal weight percentages (2.99-3.06 %wt). Furthermore, the weight percentage ratio between the elements O and Si (%wtO: %wtSi) decreased as the calcination temperature increased, specifically 2.82 for MZ@300, 0.53 for MZ@500, and 0.37 for MZ@700 (Figure 2d).

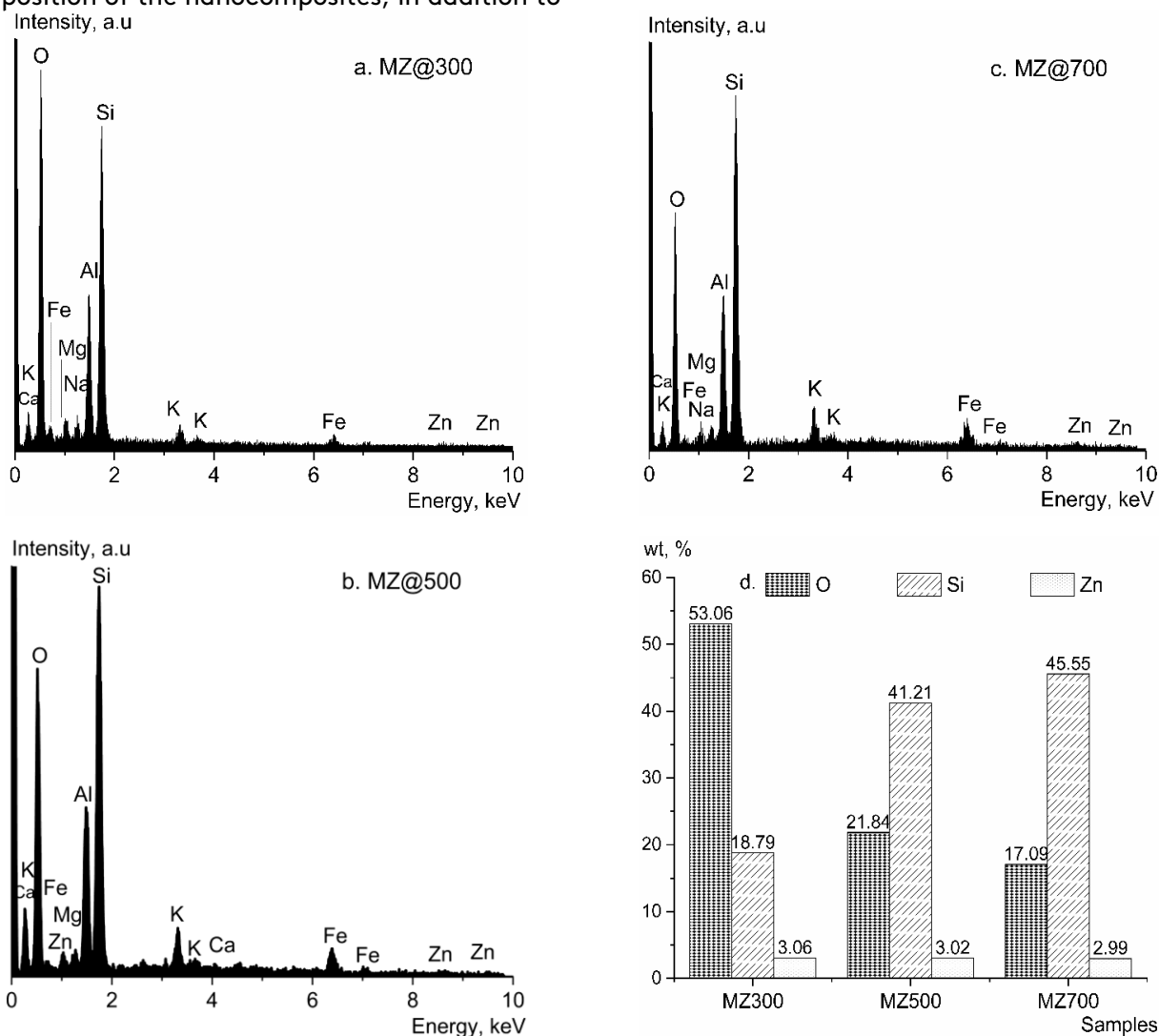


Fig. 2. EDX spectrum of MZ@300, MZ@500, and MZ@700.

XRD studies were conducted to investigate the influence of annealing temperature on the crystallization of the structure, as depicted in Figure 3. The results suggested that when annealed within the range of 300-500°C, the crystallization of ZnO appeared to remain unchanged compared to commercial ZnO. All ZnO samples at 300, 500, and 700°C exhibited a wurtzite hexagonal phase structure with well-defined diffraction peaks at angles of 31.5, 34.4, 36.2, 47.5, 56.6; 63.1, 66.4,

68.1, 69.3, 72.6, and 77.2 degrees. These scattering angles corresponded to the respective reflection planes (100), (002), (101), (102), (110), (103), (200), (112), (201), (004), and (202), closely matching with the JCPDS standard data number JCPDS 36-1451 and references [17, 29, 30]. The intensity of the peaks along the (100), (002), and (101) planes consistently increased as the annealing temperature was raised from 300-700°C, indicating a clear improvement in crystallinity at

higher annealing temperatures. As the annealing temperature was raised, both the particle size and the crystallite size of ZnO increased (Table 1) [29, 30]. The particle size was extracted from the FESEM images, the crystallite size was computed from XRD patterns employing the Debye-Scherrer equation, and the full-width at half-maximum (FWHM) was determined using Origin software. At room temperature, the XRD pattern of MMT exhibited a characteristic (001) reflection at a diffraction angle of 6.2° . The interlayer spacing of MMT, calculated using formula (1), was 14.4 \AA , equivalent to that of commercial MMT found in references [31-33].

The XRD pattern of the MMT and ZnO nanocomposites at various annealing temperatures can be divided into three regions: MMT ($2\theta \sim 5\text{-}16^\circ$), SiO_2 ($2\theta \sim 16\text{-}30^\circ$), and wurtzite hexagonal ($2\theta \sim 30\text{-}37^\circ$). From 500°C downwards, the X-ray diffraction peak (001) of MMT tended to shift towards higher 2θ angles, and the d_{001} spacing decreased from 14.4 \AA to 11.3 \AA (MZ@300) and 9.8 \AA (MZ@500) [34, 35]. During the annealing process, the interlayers became more ordered, and the crystal structure became more ordered as well. The amount of water molecules between the MMT layers decreased, reducing the distance between the layers [35]. At temperatures up to 700°C , the X-ray diffraction peak (001) of MMT became very weak, and the d_{001} spacing was only 9.2 \AA . This resulted from the collapse of the interlayer structure due to the decomposition of unstable MMT components (aluminosilicate crystal), leading to the breakdown of the crystal layers [35]. The wurtzite hexagonal phase of ZnO (2θ angle $\sim 30\text{-}37^\circ$) in MMT/ZnO had low intensity due to the low content of ZnO in the nanocomposite.

$$d_{hkl} = \frac{\lambda}{2\sin\theta} \quad (2)$$

where d_{hkl} (\AA) is the distance between parallel planes of MMT, λ is the radiation wavelength (1.5406 \AA), and θ (rad) is the scattering (Bragg) angle.

The surface texture of MMT and its nanocomposites was determined using nitrogen adsorption-desorption isotherms and is illustrated in Figure 4. MMT, MZ@300, MZ@500, and MZ@700 exhibited hysteresis loops characteristic of type IV isotherm-

desorption curves, with all hysteresis loops falling into the H4 category according to the IUPAC (the International Union of Pure and Applied Chemistry) classification. This indicated that the nanocomposites of MMT and ZnO fall under the category of mesoporous and medium mesopore materials, possessing open slit-shaped pores within plate-like particles. Table 2 provides a summary of the specific surface area, pore size, and pore volume parameters of MMT, MZ@300, MZ@500, and MZ@700 obtained through BET and the BJH method (Barrett-Joyner-Halenda). The textural properties of raw MMT were significantly improved upon modification with ZnO, except for MZ@700. Consequently, MZ@300 and MZ@500 displayed a more open and less ordered pore structure on their surface. The interlayer spaces of MMT, with intermediate pores, were obstructed by ZnO nanoparticles, resulting in a reduction in pore size.

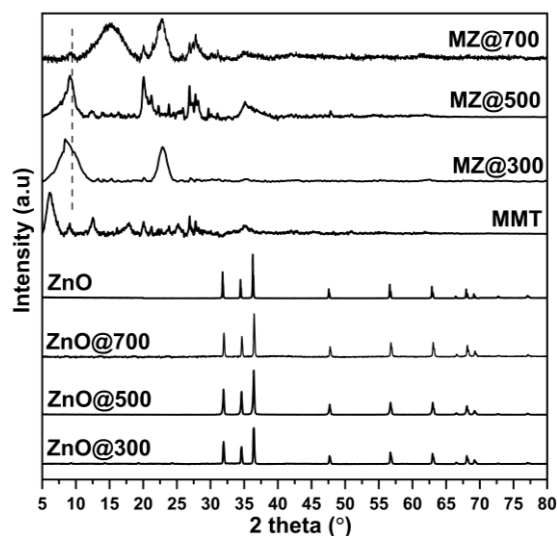


Fig. 3. XRD patterns of MMT, ZnO, ZnO@300, ZnO@500, ZnO@700, MZ@300, MZ@500, and MZ@700.

Table 1. The variation in particle size and crystallite size of ZnO with annealing temperature.

Samples	Annealing Temperature ($^\circ\text{C}$)	Particle size (nm) (From FESEM)	Crystallite size (nm) (From XRD)
ZnO@300	300	50-100	0.82
ZnO@500	500	120-200	0.93
ZnO@700	700	400-500	1.2

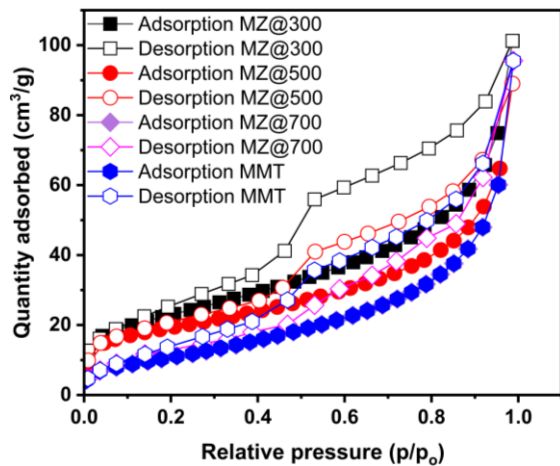


Fig. 4. N_2 adsorption-desorption isotherms of MMT, MZ@300, MZ@500, and MZ@700.

Table 2. Textural characteristics of MMT, MZ@300, MZ@500, and MZ@700.

Samples	BET surface area (m^2/g)	The pore volume (cm^3/g)	The pore size (\AA)
MMT	83.2	0.134	40.910
MZ300	134.154	0.169	39.324
MZ500	144.108	0.155	35.634
MZ700	69.433	0.116	20.582

Figure 5 is the FTIR spectrum, illustrating the bond vibrations of MMT, ZnO, ZnO@300, ZnO@500, ZnO@700, MZ@300, MZ@500, and MZ@700. At 300°C, ZnO@300 exhibited clearly defined absorption peaks at 565, 1410, 1664, and 3551 cm^{-1} [34-36]. The Zn-O stretching vibration confirmed the formation of ZnO, which appeared most prominently at 565 cm^{-1} and became more pronounced at higher calcination temperatures [37]. The vibrational mode of the Zn-O bond occurred at 1410 cm^{-1} [38]. The O-H bond of physisorbed water and the O-H bond of the water molecules adsorbed on the surface of the ZnO vibrations corresponded at a short band at 1664 cm^{-1} and a small and wide band at 3551 cm^{-1} , respectively [39]. The O-H bonds weakened gradually as the annealing temperature increased due to the evaporation process. MMT exhibited characteristic vibrations: a symmetric stretching

vibration of Al-O-Si at the wavenumber of 524 cm^{-1} [40]; at 1080 cm^{-1} , it was characteristic of the asymmetric stretching vibration of Si-O; the vibration at 1640 cm^{-1} was characteristic of the deformation vibration of H-O-H within the interlayers; and the vibrations at 3388 cm^{-1} and 3621 cm^{-1} were characteristic of the symmetric stretching vibrations of -OH groups from the water molecules incorporated into the MMT structure. Notably, there was a competition of vibrations between the range of 565 cm^{-1} and 1080 cm^{-1} in MMT/ZnO nanocomposites. At 700°C, the intensity of both bonds at 565 cm^{-1} and 1080 cm^{-1} was weak, attributed to the decomposition of unstable MMT components and the weak bonding of Zn-O within the nanocomposite.

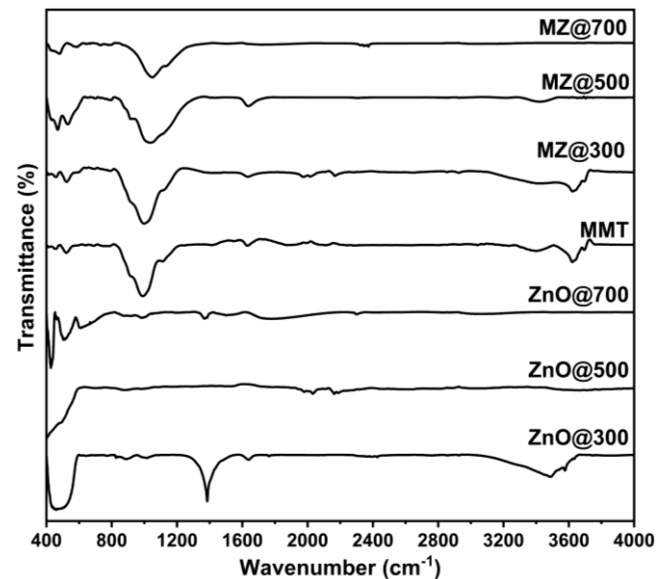


Fig. 5. FTIR spectra of MMT, ZnO, ZnO@300, ZnO@500, ZnO@700, MZ@300, MZ@500, and MZ@700.

3.2. Photocatalytic degradation test

The photocatalytic degradation efficiency of rhB over time in the presence of different photocatalysts, namely MMT, ZnO@300, ZnO@500, ZnO@700, MZ@300, MZ@500, and MZ@700, is described in Figure 6. All mixtures of each type of photocatalyst and the rhB solution were stirred in the dark for 60 minutes to establish an adsorption-desorption equilibrium. It is evident that all ZnO samples within the temperature range of 300 to 500°C did not exhibit adsorption capabilities due to the inherent nature of this metal

oxide, and their efficiency only changed when stimulated by UVC radiation. On the contrary, MMT only exhibited adsorption properties ($H_{ads} = 57\%$), and it seemed to lack photocatalytic activity as the performance remained relatively constant during irradiation. When exposed to UVC radiation, the overall performance of all ZnO samples within the annealing temperature range of 300-500°C improved; however, it was still insufficient for efficient rhB degradation. At an annealing temperature of 700°C, MZ@700 hardly showed any adsorption or photocatalytic capability because the lattice structure of MMT was disrupted, reducing its swelling and adsorption capacity. Meanwhile, MZ@500 and MZ@300 exhibited high total performance, almost completely decolorizing rhB ($H\%_{MZ@500} = 95.5\%$ and $H\%_{MZ@300} = 99.0\%$). This decolorization performance was comparable to that reported in other studies (Table 3). Additionally, the catalysts used in this research also contributed to reducing the energy source requirements and the amount of catalyst needed. Notably, even though the adsorption performance of MZ@300 was relatively high ($H_{ads}\% = 79\%$) compared to MZ@500 ($H_{ads}\% = 40\%$), the photocatalytic performance of MZ@300 ($HPC\% = 20\%$) was significantly lower than that of MZ@500 ($HPC\% = 55.5\%$). The rhB molecules, after being adsorbed on the surface of MMT, simultaneously became active sites for the photocatalytic process. The energy from UVC radiation excited electrons from the valence band to the conduction band of ZnO, creating electron-hole pairs. Normally, recombination would occur soon after; however, the d orbitals of the metallic elements in MMT trapped these electron-hole pairs to prevent recombination [41, 42]. Subsequently, the photo-oxidation and photoreduction processes took place in the valence and conduction bands of ZnO, respectively, generating free radicals (h^+ , $\bullet OH$, and $\bullet O_2^-$) to degrade the rhB molecules [43-45]. The excessive adsorption of rhB molecules onto the surface of the photocatalyst material hindered the path of incoming rays and reduced the degradation efficiency of MZ@300.

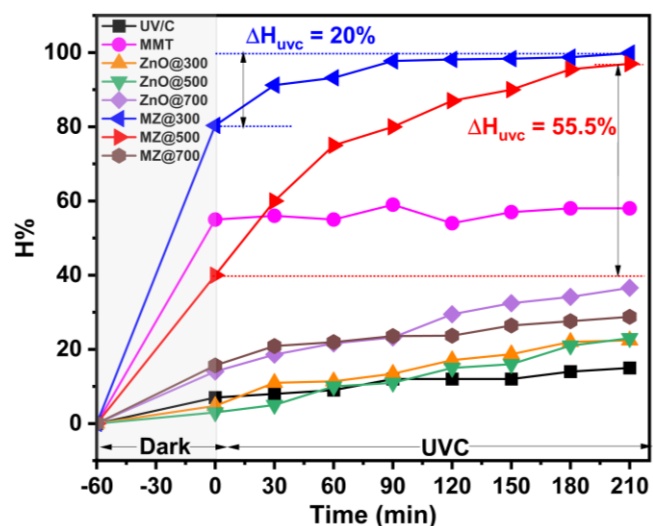
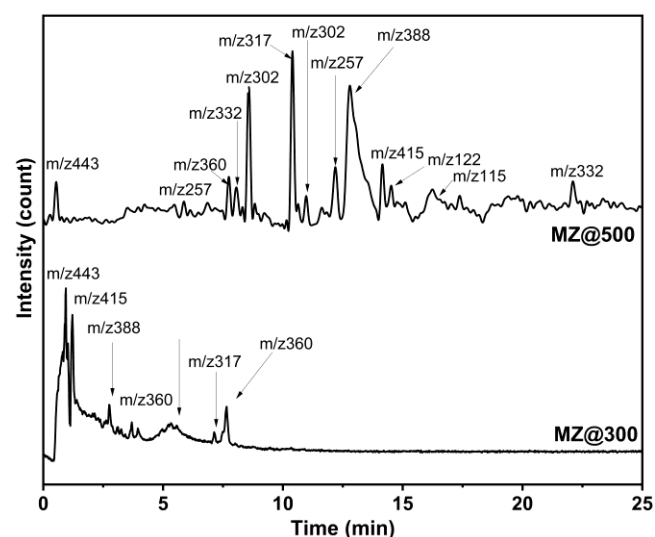


Fig. 6. Photocatalytic degradation test for 210 min of irradiation time.

The intermediate compounds were identified using the LCMS method, as shown in Figure 7. Accordingly, the rhB solution (m/z 443) was fragmented into smaller molecular weight compounds, referred to as byproducts of the photocatalytic process. Due to the lower photocatalytic efficiency of MZ@300 compared to MZ@500, there were fewer byproducts generated in MZ@300 than in MZ@500. The N-demethylation process (involving compounds N, N, N-diethyl-N'-ethyl rhodamine (m/z 415), N, N-diethyl rhodamine (m/z 388), and N'-monomethyl-ethyl rhodamine (m/z 360)) and the cleavage of the chromophore structure of rhB (involving compounds N, N-diethyl rhodamine (m/z 332) [54-55], N, N'-ethyl rhodamine (m/z 332), N'-ethyl rhodamine (m/z 317) [56-57], 2-(3H-xanthen-9-yl) benzoic acid (m/z 302) [58, 59], 2-(3-hydroxy-6-oxoxanthen-9-yl)benzoic acid (m/z 302), and 9-phenyl-3H-xanthen-9-yl) [60, 61] all occurred in both MZ@300 and MZ@500. In particular, the ring-breaking process, involving active species like h^+ , $\bullet OH$, and $\bullet O_2^-$ attacking the carbon centers concentrated within RhB molecules and oxidizing them into lower molecular weight byproducts, only occurred with MZ@500 (including the compounds benzoic acid (m/z 123) and malonic acid (m/z 115)) [62, 63]. Thus, this study demonstrated that 500°C was the appropriate annealing temperature for forming the MMT/ZnO nanocomposite, making it highly effective for decolorizing and degrading the organic dye rhB.

Table 3. Assessing the photocatalytic efficacy of MMT/ZnO in the degradation of rhodamine B in comparison to previous studies.

Photocatalyst	Calcination temperature (°C)	Concentration of RhB (ppm)	Light source	Photocatalyst amount (g/L)	Efficiency (%)	Exposition time (min)	Ref.
MMT/ZnO	500	10	UVC lamp (15 W)	0.1	95.5	210	This study
ZnO-MMT	500	10	UVC lamp (10 W)	0.1	57.4	300	[46]
Bi-doped TiO ₂ /MMT	600	10	LED lamp (100W)	0.05	88,16	150	[47]
SnO ₂ /MMT	600	50	ultrasonic power (68 W)	0.5	100	120	[48]
Zeolite Socony Mobil-5 incorporated ZnO	550	10	tungsten lamp (40W)	0.5	98.5	180	[49]
ZnO@WO ₃	120	10	xenon lamp (350W)	0.5	98	90	[50]
ZnFe ₂ O ₄ @ZnO	500	5	LED lamps (30W) six UV tubes (36W/ tube)	0.75	91.87	240	[51]
ZnO nanoparticles	550	25	halogen lamp (100W)	2	95	70	[52]
ZnO/GO	400	10	halogen lamp (100W)	0.5	97.7	60	[53]

**Fig. 7.** Intermediate products of RhB degradation over MZ@300 and MZ@500.

The photocatalytic degradation experiments of rhB were conducted sequentially to evaluate the

stability of MZ@500, as illustrated in Figure 8. After the initial testing cycle, the photocatalyst material was centrifuged, thoroughly washed, dried, and then reintroduced into the RhB solution for the subsequent photocatalytic cycle. This process was repeated similarly for the following testing cycles. The results showed that the photocatalytic degradation performance decreased by 20% after three testing cycles. After each run, rhB molecules were adsorbed on the surface of the photocatalyst material and were not completely removed, which was the reason for the reduced performance in subsequent runs.

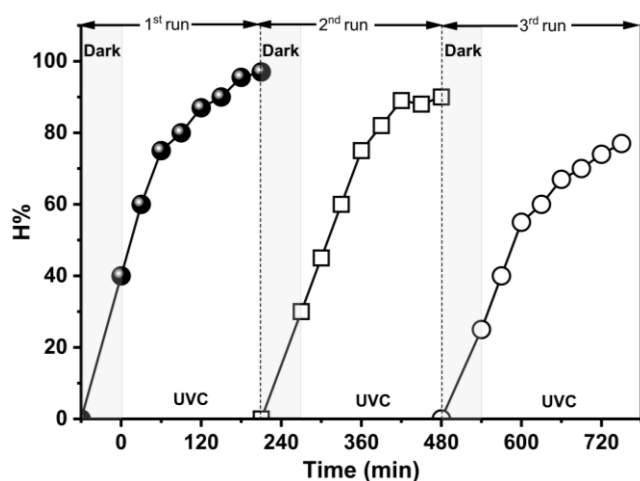


Fig. 8. Photocatalytic activity of MZ@500 for three consecutive runs.

4. Conclusion

Rhodamine B, a member of the azo dye group, is well-known for its high resistance to degradation and harmful effects on living organisms. The current trend in material development focuses on creating environmentally friendly and highly efficient photocatalysts derived from natural sources. In line with this trend, our research involved the synthesis of a Montmorillonite/ZnO nanocomposite using a combination of chemical and thermal methods within a temperature range of 300 to 700°C. The study's findings revealed that the MMT/ZnO nanocomposite exhibited the highest performance in degrading Rhodamine B at a calcination temperature of 500°C. At this temperature, the composite not only demonstrated superior photocatalytic activity but also effectively cleaved the dye's colored structure. This research underscores the potential of MMT/ZnO nanocomposites as sustainable and effective solutions for the degradation of persistent organic dyes like Rhodamine B.

Acknowledgment

This research was funded by the University of Science, VNU-HCM, under grant number T2023-72. The authors are grateful for this financial support. This work was also supported by the Materials Fundamental Laboratory-Faculty of Materials Science and Technology from the University of Science, VNU-HCM.

References

- [1] Ha Thuc, C. N., Grillet, A-C., Duclaux, L., Reinert, L., Ha Thuc, H. (2010). Separation and purification of montmorillonite and polyethylene oxide modified montmorillonite from Vietnamese bentonites. *Applied Clay Science*, 49 (3), 229-238. <https://doi.org/10.1016/j.clay.2010.05.011>
- [2] Yujin, B., Chanyoung, S., Taehyun, Y., Yongsun g, J., Ho, Y. J. (2023). Prediction of Na- and Ca-montmorillonite contents and swelling properties of clay mixtures using Vis-NIR spectroscopy. *Geoderma*, 430, 116294. <https://doi.org/10.1016/j.geoderma.2022.116294>
- [3] Ha Thuc, C. N., Cao, H. T., Nguyen, M. D., Tran., M. A., Laurent, D., Anne-Cecile, G., Ha Thuc, H. (2014). Preparation and Characterization of Polyurethane Nanocomposites Using Vietnamese Montmorillonite Modified by Polyol Surfactants. *Journal of Nanomaterials*, 12, 302735. <https://doi.org/10.1155/2014/302735>
- [4] Sunki, K., Jongmyoung, L., Donghoon, S., Youn gjin, C., Byungkyu, P. (2023). Comparative study of the cesium adsorption behavior of montmorillonite and illite based on their mineralogical properties and interlayer cations. *Journal of Hazardous Materials Advances*, 10, 100258. <https://doi.org/10.1016/j.hazadv.2023.100258>
- [5] Nguyen, V. H., Chu, V. H., Luu, T. H., Vo Nguyen, D. K., Ha Thuc, C. N. (2020). The starch-modified montmorillonite for the removal of Pb (II), Cd (II), and Ni(II) ions from aqueous solutions. *Arabian Journal of Chemistry*, 13, 7212-7223. <https://doi.org/10.1016/j.arabjc.2020.08.003>
- [6] Zhi-lei, Z., Chuang, Y., Rao-ping, L., Xiaoqing, C., Zhihao, C., Zhaokai, Y., Ze-xiang, W. (2023). Preparation and characterization of sodium polyacrylate grafted montmorillonite nanocomposite for the adsorption of cadmium ions from aqueous solution. *Colloids and Surfaces A: Physicochemical and Engineering Aspects*, 656 (B), 130389.

- <https://doi.org/10.1016/j.colsurfa.2022.130389>
- [7] Sen, Y., Gang, Y. (2023). Origin for superior adsorption of metal ions and efficient control of heavy metals by montmorillonite: A molecular dynamics exploration. *Chemical Engineering Journal Advances*, 14, 100467. <https://doi.org/10.1016/j.ceja.2023.100467>
- [8] Miguel, A., López, Z., Bernardo, F. B. (2022). Montmorillonite-perlite-iron ceramic membranes for the adsorption/removal of As (III) and other constituents from surface water. *Ceramics International*, 48 (21), 31695-31704. <https://doi.org/10.1016/j.ceramint.2022.07.091>
- [9] Min-min, W., Li, W. (2013). Synthesis and characterization of carboxymethyl cellulose/organic montmorillonite nanocomposites and its adsorption behavior for Congo Red dye. *Water Science and Engineering*, 6 (3), 272-282. <https://doi.org/10.3882/j.issn.1674-2370.2013.03.004>
- [10] Sirajudheen, P., Karthikeyan, P., Basheer, M. C., Meenakshi, S. (2020). Adsorptive removal of anionic azo dyes from effluent water using Zr(IV) encapsulated carboxymethyl cellulose-montmorillonite composite. *Environmental Chemistry and Ecotoxicology*, 2, 73-82. <https://doi.org/10.1016/j.enceco.2020.04.002>
- [11] Sedigheh, A., Maryam, H. (2017). Variation of the photocatalytic performance of decorated MWCNTs (MWCNTs-ZnO) with pH for photodegradation of methyl orange. *J Mater Sci: Mater Electron.*, 28, 11846-11855. <https://doi.org/10.1007/s10854-017-6992-5>
- [12] Sedigheh, A., Maryam, H., Mehri-Saddat, E. K. (2017). Removal efficiency optimization of organic pollutant (methylene blue) with modified multi-walled carbon nanotubes using design of experiments (DOE). *J. Mater Sci: Mater Electron.*, 28, 9900-9910. <https://doi.org/10.1007/s10854-017-6745-5>
- [13] Mehdi, A. K., Susmita, S., Krishna G., Bhattacharyya, G., Dhruva C. (2022). Montmorillonite and modified montmorillonite as adsorbents for removal of water-soluble organic dyes: A review on current status of the art. *Inorganic Chemistry Communications*, 143, 109686. <https://doi.org/10.1016/j.inoche.2022.109686>
- [14] Nandana, C., Prabhat, R., Anand, G. C., Parag, R. G. (2023). Performance comparison of photocatalysts for degradation of organic pollutants using experimental studies supported with DFT and fundamental characterization. *Catalysis Communications*, 174, 106589. <https://doi.org/10.1016/j.catcom.2022.106589>
- [15] Sedigheh, A., Mehri-Saddat, E.K., Mostafa, T. (2017). Modeling and predicting the photodecomposition of methylene blue via ZnO-SnO₂ hybrids using design of experiments (DOE). *J Mater Sci: Mater Electron*, 28 (3). <https://doi.org/10.1007/s10854-017-7414-4>
- [16] Amir, H. N., Mohammad, F., Mostafa, T., Sedigheh, A. (2019). Novel photocatalytic coatings based on tin oxide semiconductor. *Surface Engineering*, 35 (3), 216-226. <https://doi.org/10.1080/02670844.2018.1477559>
- [17] Dao, T. B. T., Ha, T. T. L., Nguyen, D. T., Le, H. N., Luu, Q. K., Nguyen, T. H., Ha-Thuc, C. N. (2023). Vietnamese Montmorillonite Supported ZnO: Preparation, Characterization and Photocatalytic Enhancement in Degradation of Rhodamine B. *Kinetics and Catalysis*, 64 (4), 390-402. <https://doi.org/10.1134/S002315842304002X>
- [18] Dao, T. B., T., Ha, T. T. L., Nguyen, T. D., Le, H. N., Ha-Thuc, C. N., Nguyen, T. M. L., Patrick, P., Nguyen, D. M. (2021). Effectiveness of photocatalyst of MMT-supported TiO₂ and TiO₂ nanotubes for rhodamine B degradation. *Chemosphere*, 280, 130802. <https://doi.org/10.1016/j.chemosphere.2021.130802>
- [19] Abbasi, S., Dastan, D., Țălu, Ș., Tahir, M., Elias, M., Lin, T., Zhi, L. (2022). Evaluation of the dependence of methyl orange organic pollutant removal rate on the amount of titanium dioxide nanoparticles in MWCNTs-TiO₂ photocatalyst using statistical methods and Duncan's multiple range test. *International Journal of Environmental Analytical Chemistry*, 248252147. <https://doi.org/10.1080/03067319.2022.2060085>
- [20] Sedigheh, A. (2023). Studying the destruction of pollutant in the presence of photocatalysts based on MWCNTs with

- controlled values of TiO₂ nanoparticles. *Applied Water Science*, 13, 100.
<https://doi.org/10.1007/s13201-023-01903-8>
- [21] Sedigheh, A., Maryam, H., Fatemeh, A., Mika, S., Davoud, D., Amine, A. (2021). Application of the statistical analysis methodology for photodegradation of methyl orange using a new nanocomposite containing modified TiO₂ semiconductor with SnO₂. *International Journal Of Environmental Analytical Chemistry*, 101 (2), 208 – 224.
<https://doi.org/10.1080/03067319.2019.1662414>
- [22] Suguna, A., Prabhu, S., Selvaraj, M., Geerthana, Geerthana, M., Silambarasan, A., Navaneethan, M., Ramesh, R., Sridevi, C. (2022). Annealing effect on photocatalytic activity of ZnO nanostructures for organic dye degradation. *Journal of Materials Science: Materials in Electronics*, 33, 8868–8879.
<https://doi.org/10.1007/s10854-021-06942-y>
- [23] Ahmad, U., Rajesh, K., Girish, K., Algarni, H., Kim, S. H. (2015). Effect of annealing temperature on the properties and photocatalytic efficiencies of ZnO nanoparticles. *Journal of Alloys and Compounds*, 648, 46-52.
<https://doi.org/10.1016/j.jallcom.2015.04.236>
- [24] Nadir, F. H., Raid, I., Husam, R. A. (2014). Effect of Annealing Temperature on the Optical Properties of ZnO Nanoparticles. *International Letters of Chemistry Physics and Astronomy*, 4, 47-47.
<https://doi.org/10.18052/www.scipress.com/ILCPA.23.37>
- [25] Najmeh, R., Sedigheh, A., Mahdieh, G. (2017). Statistical analysis of the photocatalytic activity of decorated multi-walled carbon nanotubes with ZnO nanoparticles. *J Mater Sci: Mater Electron*, 28, 6047–6055.
<https://doi.org/10.1007/s10854-016-6280-9>
- [26] Najmeh, R., Sedigheh, A., Mahdieh, G. (2017). The experimental and statistical investigation of the photo degradation of methyl orange using modified MWCNTs with different amount of ZnO nanoparticles. *J Mater Sci: Mater Electron*, 28, 7343-7352.
<https://doi.org/10.1007/s10854-017-6421-9>
- [27] Redouane, H., Hamza, I., Rahime, E., M., Said, A., Fadi, A., Eman, A., Huda, A., Hassan, O., Abdelaziz, A. A., Amane, J. (2023). Exploring ZnO/Montmorillonite photocatalysts for the removal of hazardous RhB Dye: A combined study using molecular dynamics simulations and experiments. *Materials Today Communications*, 35, 105915.
<https://doi.org/10.1016/j.mtcomm.2023.105915>
- [28] Jixiang, X., Jianyang, G., Wenbo, W., Chao, W., Lei, W. (2018). Noble metal-free NiCo nanoparticles supported on montmorillonite/MoS₂ heterostructure as an efficient UV-visible light-driven photocatalyst for hydrogen evolution. *International Journal of Hydrogen Energy*, 43 (3), 1375-1385.
<https://doi.org/10.1016/j.ijhydene.2017.11.129>
- [29] Sedigheh, A., Fatemeh, A., Mohammad, I., MehriSaddat, E. K. (2020). Synthesis of magnetic Fe₃O₄@ZnO@graphene oxide nanocomposite for photodegradation of organic dye pollutant. *International Journal Of Environmental Analytical Chemistry*, 100(2), 225 – 240.
<https://doi.org/10.1080/03067319.2019.1636038>
- [30] Ahmad, U., Rajesh, K., Girish, K., Algarni, H., Kim, S. H. (2015). Effect of annealing temperature on the properties and photocatalytic efficiencies of ZnO nanoparticles. *Journal of Alloys and Compounds*, 648, 46-52.
<https://doi.org/10.1016/j.jallcom.2015.04.236>
- [31] Irshad, A., Yanhong, Z., Jiaying, Y., Yuyu, L., Shazia, S., Muhammad, Y. N., Humaira, H., Waheed, Q. K., Khalid N. R. (2023). Semiconductor photocatalysts: A critical review highlighting the various strategies to boost the photocatalytic performances for diverse applications. *Advances in Colloid and Interface Science*, 311, 102830.
<https://doi.org/10.1016/j.cis.2022.102830>
- [32] Is, F., Sesy, A., Imam, S., Gani, P., Suresh, S., Ruey-An, D. (2021). Visible light sensitized porous clay heterostructure photocatalyst of zinc-silica modified montmorillonite by using tris (2,2'-bipyridyl) dichlororuthenium. *Applied Clay Science*, 204, 106023.

- <https://doi.org/10.1016/j.clay.2021.106023>.
- [33] Li, Z., Chitiphon, C., Vellaichamy, B., Karthikeyan, S., Bunsho, O., Keiko, S. (2022). Determination of the roles of FeIII in the interface between titanium dioxide and montmorillonite in FeIII-doped montmorillonite/titanium dioxide composites as photocatalysts. *Applied Clay Science*, 227, 106577.
<https://doi.org/10.1016/j.clay.2022.106577>
- [34] Zhenshi, S., Yingxu, C., Qiang, K., Ye, Y., Jun, Y. (2002). Photocatalytic degradation of cationic azo dye by TiO₂/bentonite nanocomposite. *Journal of Photochemistry and Photobiology A: Chemistry*, 149 (1-3), 169-174.
[https://doi.org/10.1016/S1010-6030\(01\)00649-9](https://doi.org/10.1016/S1010-6030(01)00649-9)
- [35] Wangbing, H., Jie, M., Changdong, L., Shengyi, Y., Xin, H., Guobin, F. (2020). Effects of Temperature on Structural Properties of Hydrated Montmorillonite: Experimental Study and Molecular Dynamics Simulation. *Advances in Civil Engineering*, 2020, 8885215.
<https://doi.org/10.1155/2020/8885215>
- [36] Walber, A. F., Barbara, E. C. F. S., Maxwell, S. R., Pollyana, T., Luzia, M. C. H., Ramón, P. G., Ana, C. S. A., Edson, C. S. F., Maria, G. F., Marcelo, B. F., Josy, A. O. (2022). Facile synthesis of ZnO-clay minerals composites using an ultrasonic approach for photocatalytic performance. *Journal of Photochemistry and Photobiology A: Chemistry*, 429, 113934.
<https://doi.org/10.1016/j.jphotochem.2022.113934>
- [37] Sedigheh, A. (2021). Response Surface Methodology for Photo Degradation of Methyl Orange Using Magnetic Nanocomposites Containing Zinc Oxide. *Journal of Cluster Science*, 32, 805-812.
<https://doi.org/10.1007/s10876-020-01847-y>
- [38] Subash, B., Sasikala, R., Jayamoorthy, K., Magesan, P. (2023). Heterojunction of Bentonite Clay supported Bi₂O₃/ZnO composite for the detoxification of azo dyes under UV-A light illumination. *Chemical Physics Impact*, 6, 100152.
<https://doi.org/10.1016/j.chphi.2022.100152>
- [39] Morteza, G., Moones, H., Amin, E. (2022). Biosynthesis of ZnO nanoparticles supported on bentonite and the evaluation of its photocatalytic activity. *Materials Research Bulletin*, 149, 111714.
<https://doi.org/10.1016/j.materresbull.2021.111714>
- [40] Hannatu, A. S., Mansor, B. A., Mohd, Z. H., Nor, A. I., Aminu, M., Tawfik, A. S. (2017). Nanocomposite of ZnO with Montmorillonite for Removal of Lead and Copper Ions from aqueous solutions. *Process Safety and Environment Protection*, 109, 97-105.
<https://doi.org/10.1016/j.psep.2017.03.024>
- [41] Sedigheh, A., Zhi, L., Davoud, D., Lin, T. (2023). The effect of individual factors, their binary and ternary interactions on photodegradation rate of organic contaminants using photocatalysts based on multi-walled carbon nanotubes (MWCNTs): statistical analysis based on ANOVA and RSM. *Environmental Monitoring and Assessment*, 195, 1191.
<https://doi.org/10.1007/s10661-023-11704-w>
- [42] Sedigheh, A. (2023). Magnetic photocatalysts based on graphene oxide: synthesis, characterization, application in advanced oxidation processes and response surface analysis. *Applied Water Science*, 13, 128.
<https://doi.org/10.1007/s13201-023-01931-4>
- [43] Sedigheh, A. (2020). Adsorption of Dye Organic Pollutant Using Magnetic ZnO Embedded on the Surface of Graphene Oxide. *Journal of Inorganic and Organometallic Polymers and Materials*, 30, 1924-1934.
<https://doi.org/10.1007/s10904-019-01336-4>
- [44] Sedigheh, A. (2019). Photocatalytic activity study of coated anatase-rutile titania nanoparticles with nanocrystalline tin dioxide based on the statistical analysis. *Environ Monit Assess.*, 191, 206.
<https://doi.org/10.1007/s10661-019-7352-0>
- [45] Sedigheh, A., Mehri-Saddat, E. K. (2019). The influence of ZnO nanoparticles amount on the optimisation of photo degradation of methyl orange using decorated MWCNTs. *Progress in Industrial Ecology – An International Journal*, 13 (1), 3-15.
<https://doi.org/10.1504/PIE.2019.098760>
- [46] Phetladda, P., Apisit, S., Weerapat, F., Pinit, K., Weekit, S. (2018). Homogeneous distribution of nanosized ZnO in montmorillonite clay sheets for the

- photocatalytic enhancement in degradation of Rhodamine B. *Research on Chemical Intermediates*, 44, 6861–6875.
<https://doi.org/10.1007/s11164-018-3526-6>
- [47] Biyang, T., Shengqing, W., Haichun, X., Jianli, W., Yuying, M. (2024). Optimization of preparation conditions of Bi-doped TiO₂/montmorillonite composites and its photodegradation of Rhodamine B. *Desalination and Water Treatment*, 100328.
<https://doi.org/10.1016/j.dwt.2024.100328>
- [48] Is, F., Rico, N., Imam, S., Ganjar, F., Bambang, H. N., Azlan, K., Oki, M. (2020). Sonocatalytic degradation of rhodamine B using tin oxide/ montmorillonite. *Journal of Water Process Engineering*, 37 (2020) 101418.
<https://doi.org/10.1016/j.jwpe.2020.101418>
- [49] Suguna, A., Sridevi, C., Parthibavarman, M., Manikandababu, C. S., Ramachandran, K., BoopathiRaja, R. (2024). Design and fabrication of Zeolite Socony Mobil-5 incorporated ZnO composite for enhanced visible light photocatalytic performance. *Chemical Physics Impact*, 8, 100621.
<https://doi.org/10.1016/j.chphi.2024.100621>
- [50] Yongxin, X., Tiwei, C. (2023). Development of nanostructured based ZnO@WO₃ photocatalyst and its photocatalytic and electrochemical properties: Degradation of Rhodamine B. *International Journal of Electrochemical Science*, 18 (4), 100055.
<https://doi.org/10.1016/j.ijoes.2023.100055>
- [51] Loan, T. T. N., Dai-Viet, N. V., Lan, T. H. N., Anh, T. T. D., Hai, Q. N., Nhuong, M. C., Duyen, T. C. N., Thuan, V. C. (2022). Synthesis, characterization, and application of ZnFe₂O₄@ZnO nanoparticles for photocatalytic degradation of Rhodamine B under visible-light illumination. *Environmental Technology & Innovation*, 25, 102130.
<https://doi.org/10.1016/j.eti.2021.102130>
- [52] Manmohan, L., Praveen, S., Lakhvinder, S., Chhotu, R. (2023) Photocatalytic degradation of hazardous Rhodamine B dye using sol-gel mediated ultrasonic hydrothermal synthesized of ZnO nanoparticles. *Results in Engineering*, 17, 100890.
<https://doi.org/10.1016/j.rineng.2023.100890>
- [53] Abdulla, S. M., Amran, M. H. S., Ishtiaque, M. S., Mahabub, A. B. (2024) Effective adsorption and visible light driven enhanced photocatalytic degradation of rhodamine B using ZnO nanoparticles immobilized on graphene oxide nanosheets. *Results in Physics*, 58, 107471.
<https://doi.org/10.1016/j.rinp.2024.107471>
- [54] Alireza, K., Murat, K., Semra, K., Samira, A. O. (2016). Preparation and characterization of ZnO/MMT nanocomposite for photocatalytic ozonation of a disperse dye. *Turkish Journal of Chemistry*, 40, 546 – 564.
<https://doi.org/10.3906/kim-1507-77>
- [55] Melike, K., Murat, K., Semra, K., Alireza, K., Atefeh, K. (2016). Sonocatalytic removal of naproxen by synthesized zinc oxide nanoparticles on montmorillonite. *Ultrasonics Sonochemistry*, 31, 250–256.
<http://dx.doi.org/10.1016/j.ultsonch.2016.01.009>
- [56] Chunhui, Z., Dongshen, T., Weihua, Y. (2019). 7 - Smectite Nanomaterials: Preparation, Properties, and Functional Applications. *Nanomaterials from Clay Minerals - A New Approach to Green Functional Materials Micro and Nano Technologies*, 335-364.
<https://doi.org/10.1016/B978-0-12-814533-3.00007-7>
- [57] Marina, M., Giuseppe, C., Giuseppe, L., Serena, R. (2020). 13 - Covalently modified nanoclays: synthesis, properties and applications. *Clay Nanoparticles-Properties and Applications Micro and Nano Technologies*, 305-333.
<https://doi.org/10.1016/B978-0-12-816783-0.00013-X>
- [58] Yating, Q., Tongjiang, P., Hongjuan, S., Li, Z., Yao, L., Can, Z. (2021). Effect Of Montmorillonite Layer Charge On The Thermal Stability Of Bentonite. *Clays and Clay Minerals*, 69, 328–338.
<https://doi.org/10.1007/s42860-021-00117-w>
- [59] Mohammad, H. H., Maryam, M. (2015). Effect of annealing temperature on optical properties of binary zinc tin oxide nanocomposite prepared by sol-gel route using simple precursors: Structural and optical studies by DRS, FT-IR, XRD, FESEM investigations. *Spectrochimica Acta Part A: Molecular and Biomolecular Spectroscopy*, 137, 267-270.
<https://doi.org/10.1016/j.saa.2014.08.031>

- [60] Sharma, G., Dionysiou, D., Sharm, S., Kumar, A., Al-Muhtaseb, A., Naushad, M., Stadler, F. (2019). Highly efficient Sr/Ce/activated carbon bimetallic nanocomposite for photoinduced degradation of rhodamine B. *Catal. Today*, 335, 437–451. <https://doi.org/10.1016/J.CATTOD.2019.03.063>
- [61] Hegazey, R., Abdelrahman, E., Kotp, Y. (2020). Facile fabrication of hematite nanoparticles from Egyptian insecticide cans for efficient photocatalytic degradation of rhodamine B dye. *J. Mater. Res. Technol.*, 9, 1652–1661. <https://doi.org/10.1016/j.jmrt.2019.11.090>
- [62] Changren, X., Zijun, T., Cong, W., Xiaqing, Y., Guoqing, Z., Huageng, P. (2018). Fabrication of In₂O₃/TiO₂ nanotube arrays hybrids with homogeneously developed nanostructure for photocatalytic degradation of Rhodamine B. *Materials Research Bulletin*, 106, 197-203. <https://doi.org/10.1016/j.materresbull.2018.05.022>
- [63] Ali, A. I., Amir, P., Moslem, F., Sahand, J., Babak, K. (2018). Photocatalytic degradation of Rhodamine B and Real Textile Wastewater using Fe-Doped TiO₂ anchored on Reduced Graphene Oxide (Fe-TiO₂/rGO): Characterization and feasibility, mechanism and pathway studies. *Applied Surface Science*, 462, 549-564. <https://doi.org/10.1016/j.apsusc.2018.08.133>

How to site this paper:



Dao, B. T. T., Hoang, V. D., Nguyen, T. D., Le, H. N., Nguyen, H. T. & Ha-Thu, Ch. (2024). The Impact of Annealing Temperature on Photocatalytic Degradation Performance of Rhodamine B by Montmorillonite/Zinc-Oxide Nanocomposite. *Advances in Environmental Technology*, 10(3), 187-201. doi: 10.22104/AET.2024.6572.1799